Eur. Phys. J. D **39**, 101–106 (2006)
DOI: 10.1140/epjd/e2006-00078-2

THE EUROPEAN PHYSICAL JOURNAL D

Antiphase dynamics of sub-nanosecond microchip Cr,Yb:YAG self-Q-switched multimode laser

J. Dong[a], A. Shirakawa, and K.-I. Ueda

Institute for Laser Science, University of Electro-Communications, 1-5-1 Chofugaoka, Chofu, Tokyo 182-8585, Japan

Received 28 June 2005 / Received in final form 23 January 2006
Published online 11 April 2006 –

Abstract. Stable two-mode, and three-mode oscillations due to the spatial hole burning effect were observed experimentally with the increase of the pump power ratio in a laser-diode pumped sub-nanosecond microchip Cr,Yb:YAG self-Q-switched multimode laser. The stability of the output pulse trains was attributed to the mode coupling through antiphase dynamics between different modes. Modified multimode rate equations including the spatial hole-burning effect in the active medium and the non-linear absorption of the saturable absorber were proposed. Numerical simulations of the antiphase dynamics of such a laser were in good agreement with the experimental data, and the antiphase dynamics were explained by the evolution of the inversion population and the bleaching and recovery of the inversion population of the saturable absorber.

PACS. 42.65.Sf Dynamics of nonlinear optical systems; optical instabilities, optical chaos and complexity, and optical spatio-temporal dynamics – 42.55.Xi Diode-pumped lasers – 42.60.Gd Q-switching

1 Introduction

The complicated behavior of multimode lasers have been well known since the early days of laser experiments. Recently complex multimode lasers dynamics have been revisited as an interesting subject for the study of nonlinear dynamics in optical systems. The nonlinear dynamics in multimode lasers include chaos and nonlinear mode coupling effects such as antiphase dynamics, etc. The antiphase state was first described by Hadley and Beasley in circuits containing N coupled Jesephson junctions, which is periodic in time with each oscillator having precisely the same waveform. However, each oscillator is shifted by $1/N$ of a period from its neighbor [1]. Similar dynamics were observed in the output of a multimode laser with an intracavity doubling crystal [2], and multimode lasers with gain or loss modulations [3]. In addition to being interesting for fabrication of compact integrated optical devices, microchip lasers are interesting systems for nonlinear dynamics studies. Indeed, microchip solid-state lasers are widely used as lasers for studying nonlinear effects such as chaos and antiphase dynamics [3–8]. It has been demonstrated that antiphase states can be used as a method for secure information encoding and transmission [9]. There are many reports on the antiphase states of continuous wave microchip lasers [3–6] and some reports on the passively Q-switched Nd:YAG lasers with Cr^{4+} [7] as saturable absorber and Yb:YAG laser with semiconductor saturable absorber mirror (SESAM) as saturable absorber, however, there is no such reports on the monolithic microchip passively Q-switched laser. Laser-diode-pumped passively Q-switched microchip solid-state lasers capable of delivering high peak power (several tens kW) at high repetition rate and nanosecond or sub-nanosecond pulse width can not only be potentially used in micromachine, remote sensing, target ranging, microsurgery, pollution monitoring, and so on [10–14], but also can be used as a compact resource for studying nonlinear dynamics. Recently, sub-nanosecond laser pulses were obtained in a laser-diode-pumped Cr,Yb:YAG microchip laser [15], the stable output pulse trains were obtained in a very compact multimode laser source. In this paper, we report experimental results of the stable pulse trains due to mode-coupling through antiphase dynamics for different longitudinal modes in laser-diode-pumped Cr,Yb:YAG microchip self-Q-switched lasers. Stable pulse trains due to classical antiphase dynamics in the two-mode oscillation regime, and stable pulse trains due to mode coupling through quasi- antiphase dynamics in the three-mode oscillation regime were observed. Modified multimode laser rate equations were proposed, including the cross-saturation effect due to the spatial hole-burning effect and the nonlinear absorption effect of the Cr^{4+} saturable absorber in the Cr,Yb:YAG crystal. The numerical solution of the rate equations was obtained and the antiphase dynamics of Cr,Yb:YAG laser at two-mode oscillation and the three-mode oscillation were reproduced. The numerical solutions are in good agreement with the experimental data.

[a] e-mail: jundong_99@yahoo.com

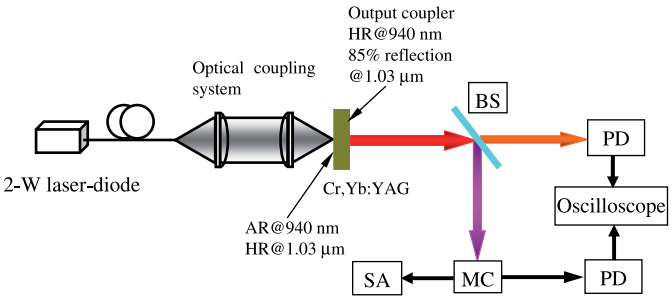

Fig. 1. Schematic of the laser-diode-pumped microchip Cr,Yb:YAG self-Q-switched laser, BS, beam splitter; PD, photodiode; MC, monochromator; SA, spectrum analyzer.

2 Experiments and results

The schematic of the laser diode pumped microchip Cr,Yb:YAG self-Q-switched laser experimental set-up is shown in Figure 1. A plane-parallel 1-mm-thick Cr,Yb:YAG crystal doped with 10 at.% Yb and 0.025 at.% Cr was used as a laser resonator. The planar rear surface was coated for high transmission (>90%) at 940 nm and total reflection (>99.9%) at 1030 nm. The planar front surface serving as output coupler was coated for 85% reflection at 1030 nm and total reflection (>98%) at 940 nm. A 2-W fiber-coupled 937.5 nm laser diode with a core diameter of 102 μm and numerical aperture of 0.15 was used as the pump source. The coupling optics (two focus lens with focal length of 8 mm) was used to focus the pump beam into the crystal rear surface. After the coupling optics, there was about 92% pump power incident on the Cr,Yb:YAG crystal and the pump light spot in Cr,Yb:YAG was about 100 μm in diameter. The Cr,Yb:YAG laser operation was performed at room temperature without cooling the Cr,Yb:YAG crystal. The Q-switched pulses were recorded by using a fiber-coupled InGaAs photodiode (Model DSC40S from Discovery Semiconductor) with a bandwidth of 16 GHz, and a Tektronix TDS7704B digital phosphor oscilloscope of 7 GHz sampling rate in the single-shot mode. The laser spectrum was analyzed using an ANDO AQ6317 optical spectrum analyzer. The laser output beam profile was monitored using a CCD camera both in the near field and far field of the output coupler, in this way the beam diameter and beam quality M^2 can be determined. In order to study the dynamics of different sets of modes separately and make sure the detected signal was one mode of the solitary laser, a monochromator was used as a wavelength band-pass filter to select different single modes. The pulse train of a selected mode and the total pulse train can be detected by using two photodiode detectors and a fast digital oscilloscope simultaneously.

The Q-switched pulses were observed when the absorbed pump power was above 680 mW, the minimum pulse width (FWHM) of 440 ps was obtained at absorbed pump power of 1500 mW. The repetition rate extended from several hundred Hz to 6.6 kHz with pump power. The output laser has a good TEM_{00} transverse intensity profile and near-diffraction-limited beam with M^2 of 1.17.

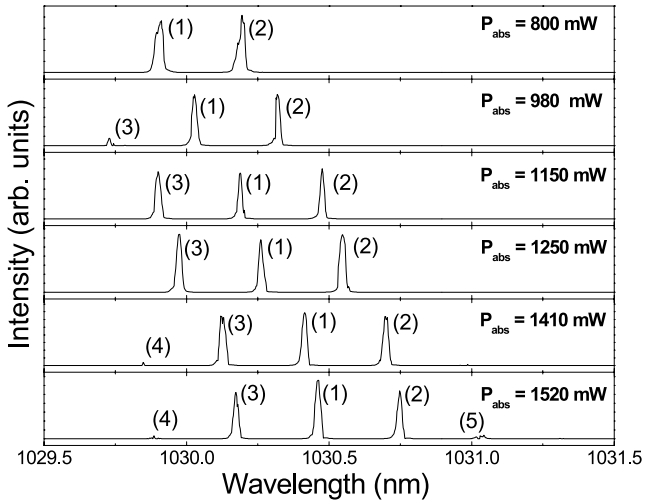

Fig. 2. Evolution of the laser spectra around 1030 nm of Cr,Yb:YAG self-Q-switched laser with absorbed pump power. The resolution of the measurement is 0.01 nm. The number in the bracket indicates the laser mode.

The maximum average output power is 156 mW and the pulse energy is 23.5 μJ when the absorbed pump power is 1520 mW. The maximum peak power is over 53 kW. The laser spectrum of this self-Q-switched laser is longitudinal multimode oscillation (around 1030 nm). The evolution of the self-Q-switched laser spectrum at different absorbed pump power is shown in Figure 2. The wavelength of each mode shifts to longer wavelengths with an increase of the absorbed pump power. This is caused by the increase of the temperature of the gain medium with increasing absorbed pump power. As the heat generated inside the gain medium increases, temperature increases and the emission spectrum of Yb:YAG crystal shifts to longer wavelengths, as indicated in reference [16]. The non-uniform temperature distribution along the radius of the gain medium induced by the pump power can also introduce cavity optical length change which will give rise to thermal lens effects and gain guiding effect in microchip lasers [17,18]. The number of lasing modes increases with the absorbed pump power. There is two-mode oscillation when the power is above threshold and w (ratio of the absorbed pump power to the absorbed pump power threshold) is below 1.4. A third mode becomes active when w is between 1.44 and 2. A fourth and fifth mode appear when w is 2.1 and w is 2.23, respectively, as shown in Figure 2. However, the intensity of the fourth-mode and fifth-mode was weaker than those of other three main oscillation modes. The fourth-mode and fifth-mode could just be the weak modes close to the threshold, i.e., amplified spontaneous emission. The contribution of these modes to the stability of the total output pulse trains can be neglected. Further increase of the absorbed pump power does not change the Q-switched laser spectrum. The separation of each frequency under different pump power is about 0.29 nm, the linewidth at each frequency is measured to be 0.02 nm by using the optical spectral analyzer with resolution of 0.01 nm. The linewidth of each mode

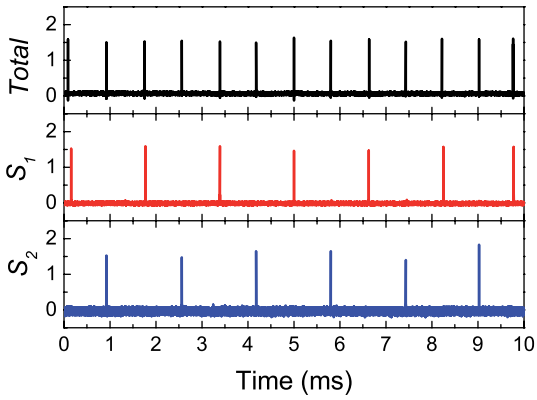

Fig. 3. The total output pulse train and the output pulse trains of each mode of self-Q-switched Cr,Yb:YAG two-mode oscillation exhibiting classic antiphase dynamics when the pump power ratio, $w = 1.2$.

would probably be narrower with a higher-resolution optical spectral instrument than used in these present measurements. According to the laser resonator theory [19], the separation of the longitudinal modes in a laser cavity is given by $\Delta\lambda = \lambda^2/2L_c$, where L_c is the optical length of the resonator. For the 1 mm Cr,Yb:YAG planar-parallel resonator studied here, $\Delta\lambda$ was calculated to be 0.2915 nm with the laser wavelength of 1030 nm, the experimental data of the space between each mode was in good agreement with the theoretical prediction.

The antiphase dynamics of the self-Q-switched Cr,Yb:YAG multimode laser was studied experimentally by measuring the contribution of each mode to the total output intensity. The measured pulse trains of each mode and the total output laser can identify the temporal behavior of the multimode laser within the antiphase regime. A typical example of the measured pulse train of self-Q-switched two-mode laser and the pulse trains of each mode is shown in Figure 3 when the pump power ratio, w, was 1.2. Two modes oscillate at nearly the same intensity. Two modes show period-1 pulsations with almost the same repetition frequency of 650 Hz. The total pulse repetition frequency, however, is 1.3 kHz, which is twice that of each mode. Comparing the total pulse repetition frequency with those of each mode, each mode is shifted from the next mode by about 1/2 of the period. This shows that the two modes operate in opposite phase, competing for the gain alternatively and display a classic antiphase state. The antiphase state of this two-mode oscillation of the microchip Cr,Yb:YAG laser is caused by the cross-saturation mechanism due to spatial hole burning coupling the modes via population gratings and the nonlinear absorption of the Cr^{4+} saturable absorber, as reported by other researchers [7]. As soon as the pump power is increased up to the three-mode regime, in which the third lasing mode began to oscillate, the mode oscillation dynamics change. The pulsations occurring for the first mode with the highest gain are characterized by a strong pulse following a weak pulse (the ratio of the weak pulse to the strong pulse is about 0.5) when the ratio of the

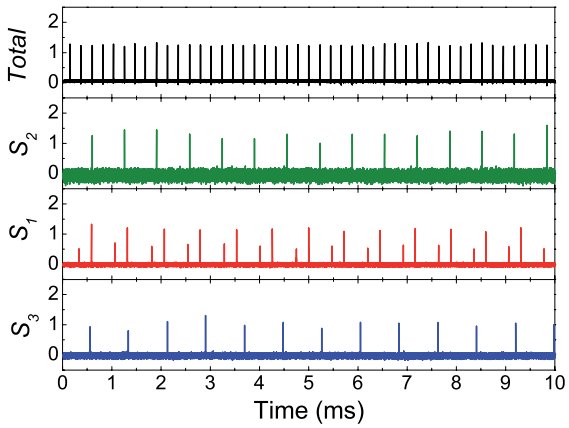

(a)

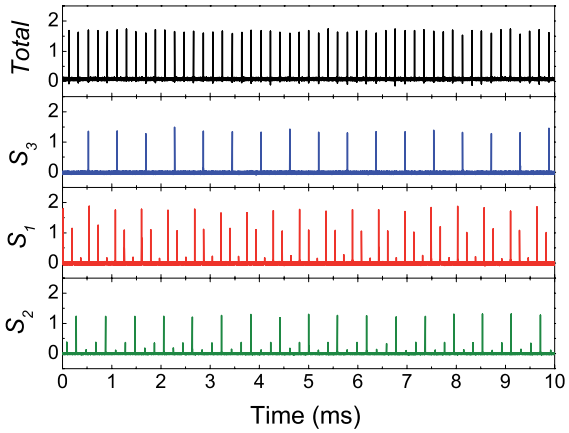

(b)

Fig. 4. The total output pulse train and the output pulse trains of each mode of self-Q-switched Cr,Yb:YAG three-mode oscillation exhibiting quasi-antiphase dynamics when the pump power ratio, (a) $w = 1.7$, (b) $w = 1.85$.

pump power, w, was 1.7 (as shown in Fig. 4a). The time interval between strong or weak pulses for the first mode is three times that for the total output pulse sequence. The pulse trains of the other two modes with lower gain are characterized as pulsation with amplitude fluctuation compared to the total output pulse train. Pulses of each mode were shifted from the next mode by one third of the period of each mode and also exhibited antiphase dynamics. With the present experimental set-up, it is difficult to obtain three separate modes oscillations simultaneously. Although there were some inaccuracies in obtaining pulse trains for each mode, the tendency of alternating oscillation of three modes was clearly observed in the experiments. These show that the stable pulse trains should be governed by mode coupling through the antiphase dynamics of different separate mode oscillations.

The Q-switched laser was still in the three-mode oscillation regime when the pump power was further increased. The output pulse train characteristics of the three-longitudinal-mode oscillation are shown in Figure 4b when the pump power ratio was 1.85. The corresponding

output pulse train of the first mode with highest gain was characterized as a weak pulse following a strong pulse. The ratio of the weak pulse to the strong pulse was about 0.6. The output pulse train of the secondary mode consisted of a strong pulse following a weak pulse; the ratio of the weak pulse to the strong pulse was about 0.2. The time interval between the strong pulses or weak pulses was 3 times that of the total output pulse train. The output pulse train of the third mode was characterized as a stable pulse output with time interval between pulses of 3 times that of the total output pulse. Therefore, when the pump power ratio was 1.85, the output pulse trains of three-mode oscillation still displayed antiphase dynamics. Actually, antiphase dynamics do not need to be periodic in each mode, and they can undergo bifurcation sequences. As the pump power was increased further, a fourth mode appeared (as shown in Fig. 2) and the repetition frequency increased. The period of the first three modes was nearly the same as those in the three-mode regime. The intensities of the fourth and fifth-mode were very small comparing to the first three modes, which means that the oscillation thresholds for these weak modes were very high comparing to the three main modes. It should be noted that the phases of the intensity pulses of individual modes are different and give rise to self-organized antiphase dynamics.

3 Numerical simulation and discussion

To fully understand the mechanics of the antiphase dynamics on the stable output pulse trains of microchip Cr,Yb:YAG multimode lasers, the modified rate equations for a passively Q-switched multimode laser of N longitudinal modes with the same transverse mode structure, including the nonlinear absorption of the saturable absorber, are introduced by taking account of the cross-saturation dynamics that are due to the spatial hole-burning effects [20], as follows:

$$\frac{dn_0}{dt} = w - n_0 - \sum_{i=1}^{N} \gamma_i \left(n_0 - \frac{n_i}{2}\right) \phi_i \tag{1}$$

$$\frac{dn_i}{dt} = \gamma_i n_0 \phi_i - n_i \left(1 + \sum_{i=1}^{N} \gamma_i \phi_i\right) \tag{2}$$

$$\frac{d\phi_i}{dt} = K\Big[\Big(\gamma_i \left(n_0 - \frac{n_i}{2}\right) - 1 - 2\left(\delta_1 N_g - \delta_2 \left(N_0 - N_g\right)\right) l\Big)\phi_i + \varepsilon n_0\Big] \tag{3}$$

$$\frac{dN_g}{dt} = \left(N_0 - N_g\right)\xi - \delta_1 N_g \sum_{i=1}^{N} \phi_i \tag{4}$$

with $i = 1, \ldots, N$. In equations (1–4), time is normalized to the fluorescence lifetime τ of the gain medium, Cr,Yb:YAG; w is the relative pump rate normalized to the first-lasing-mode absorbed pump power threshold; n_0 is the space average of the population inversion density normalized to the first-lasing-mode threshold population inversion density, n_i is the normalized Fourier component of the population inversion density for the ith mode normalized to the first-lasing-mode threshold population inversion density, which can be described as follows:

$$n_0 = \frac{1}{L_c} \int_0^{L_c} n\left(z,t\right) dz \tag{5}$$

$$n_i = \frac{2}{L_c} \int_0^{L_c} n\left(z,t\right) \cos\left(2k_i z\right) dz \tag{6}$$

where k_i is the wave number of mode i and L_c is the length of the cavity filled with active medium; ϕ_i is the normalized photon density, $\gamma_i \leq 1$ is the relative gain with respect to the first lasing mode, $K = \tau/\tau_c$ is the lifetime ratio of the fluorescence lifetime of the gain medium and the photon lifetime inside the laser cavity, l is the length of the saturable absorber, ε is the spontaneous emission coefficient, δ_1 and δ_2 are respectively the ratios of the ground absorption cross-section and the excited state absorption cross-section of the Cr^{4+} saturable absorber to the stimulated emission cross-section of the gain medium of Yb^{3+}. N_g, N_0 are the population inversion density and the total population density of Cr^{4+} saturable absorber normalized to the first-lasing-mode threshold. ξ is the ratio of the fluorescence lifetime of the gain medium to the lifetime of the saturable absorber.

Table 1. The parameters of Cr,Yb:YAG used in the numerical simulations [21].

Parameters	Value
σ	2.5×10^{-20} cm^2
σ_g	4.6×10^{-18} cm^2
σ_e	8.2×10^{-19} cm^2
τ	584 μs
τ_g	3.4 μs
K	1.5×10^7
N_0	3.37×10^{-3}
δ_1	200.87
δ_2	35.7
l	1 mm
ξ	172
ε	1.2×10^{-7}

Because the gain spectrum of Yb^{3+} in YAG crystal is sufficiently broad (about 9 nm at room temperature [16]) compared with the longitudinal mode space (0.3 nm), the gain, loss and spontaneous emission rate are assumed to be the same for all modes in the following numerical simulations. A typical numerical example of the population inversion density of the saturable absorber and the population inversion density of two modes, $n_0 - n_1/2$, $n_0 - n_2/2$, and the photon density for two-mode oscillation is shown in Figure 5. The pump rate $w = 1.2$, $\gamma_1 = 1$, $\gamma_2 = 0.99$, and the other laser parameters [21] used are listed in Table 1. ϕ_1 and ϕ_2 are the photon density of the two modes, respectively. The $n_0 - n_1/2$ value in the figure is the population inversion for the first-mode oscillation and $n_0 - n_2/2$ is the population inversion for the second-mode oscillation.

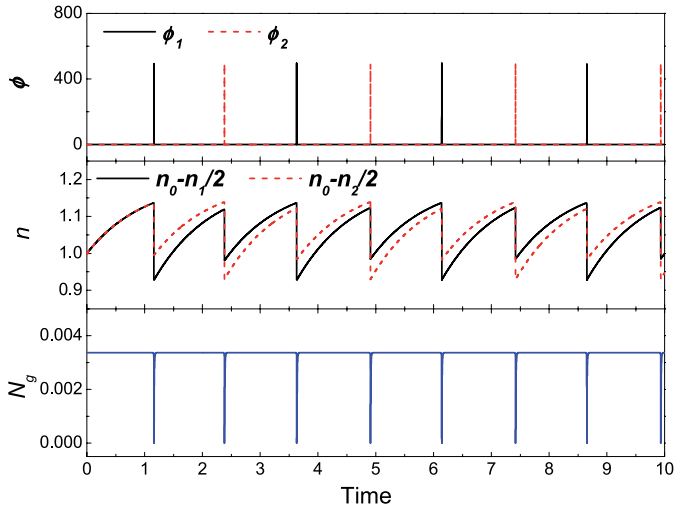

Fig. 5. Numerical simulation of the pulse sequences, the population inversion of each mode and the population inversion of the saturable absorber for two-mode antiphase dynamics when the pump power ratio, $w = 1.2$.

N_g is the inversion population of the saturable absorber. This numerical solution of two-mode oscillation is quite similar to the experimental result shown in Figure 3. The maximum output intensity in one mode is shifted 1/2 period of the repetition frequency from that of the other mode, which shows a classic antiphase state. The antiphase states were reproduced in the numerical calculations irrespective of the initial conditions for the mode intensities and gains, the antiphase state generally exists at the two-mode oscillation regime. The mechanics of the alternative antiphase pulse oscillation of Cr,Yb:YAG self-Q-switched laser under continuous-wave pumping can be explained from Figure 5 as follows [3]. The time interval between the pulses is mainly governed by the buildup time of the population inversion n to reach the threshold value, and also by the growth time of the photon density ϕ, which is very short compared to the buildup time of the population inversion, after n exceeds the threshold. Under continuous-wave pumping, the first mode of highest gain will reach its threshold first while the oscillations of the second mode are suppressed. Therefore, the decrease of the population inversion $n_0 - n_1/2$ of the first mode, just after the oscillation, is more significant than that of $n_0 - n_2/2$ for the second mode. Then, the recovery time of the population inversion for the second mode to its threshold value is shorter than that for the first mode, and the second mode oscillation suppresses the first mode. The laser pulses of the two-mode oscillate alternately under continuous-wave pumping and the nonlinear absorption of the saturable absorber; the delay time of each mode is determined by the nonlinear absorption of the saturable absorber. Similar antiphase behaviors of two-mode oscillation have been obtained generally for appropriate parameter w from 1.01 to 1.4. The numerical simulations of the population inversion density of the saturable absorber and the population inversion density of three modes, $n_0 - n_1/2$, $n_0 - n_2/2$, $n_0 - n_3/2$ and the photon density for the three-

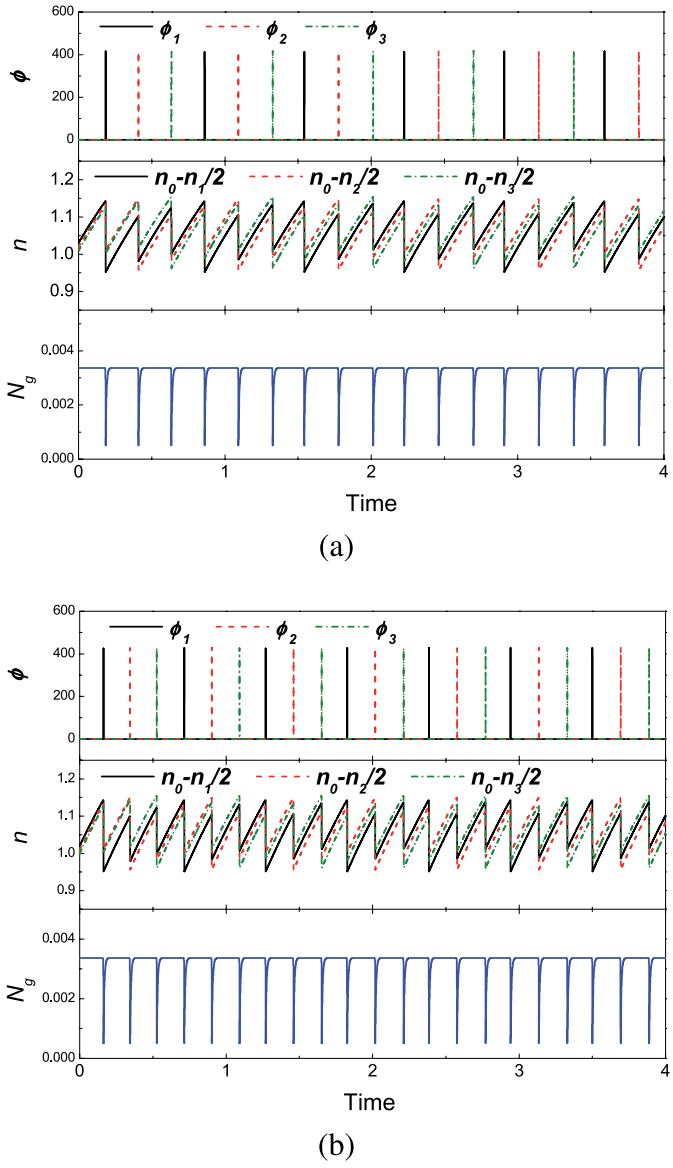

Fig. 6. Numerical simulation of the pulse sequences, the population inversion of each mode and the population inversion of the saturable absorber for three-mode oscillation under different pump power ratio (a) $w = 1.7$, (b) $w = 1.85$.

mode oscillations with $\gamma_1 = 1$, $\gamma_2 = 0.99$, $\gamma_3 = 0.98$ under different pumping power ratio are showing in Figure 6, which are similar to the experimental results shown in Figure 4. The evolution of the inversion population density with time shows that the inversion population of the three modes increases with time under continuous-wave pumping. The first mode with highest gain reaches the threshold first, and suppresses oscillations of the other modes. Then the saturable absorption is bleached under the highest gain of the first mode, the Q-switched pulse of the first mode is developed and the population inversion of the gain is depleted drastically for the first mode compared to the other modes. The inversion population of the three modes increases with continuous-wave pumping. The inversion population of the second mode will reach the threshold

first because the final state inversion population is higher than that for the first- and third-mode, and then oscillation of the first- and third-modes are suppressed. As soon as the laser pulse of the second-mode is released, the inversion population of the second-mode, $n_0 - n_2/2$ depletes significantly comparing to the third- and first-mode. At this time the third mode has the highest final-state inversion population, and will reach the threshold first whereupon the laser pulse of the third mode is released. The three modes oscillate alternately each mode shifts 1/3 of the period from the other and shows typical antiphase dynamics. The antiphase dynamics of three modes dose not change with increasing pump power. However, the time interval between the pulses will be shortened with increasing pump power, as shown in Figure 6. The time interval between each pulse for the total output is governed by the bleaching and recovery time of the population inversion of the Cr^{4+} saturable absorber. There are some discrepancies between the experimental results of the measured pulse trains of first-mode, second-mode and the numerical calculations for three-mode oscillation comparing Figure 4 with Figure 6. We assumed that the total loss of the cavity for each mode is the same during the numerical calculations, however, the loss for each mode is different in the experiments, and the mode oscillation becomes complicated with the pump power as shown in Figure 4. There is two-pulse as a group for the first-mode oscillation when the pump power ratio is 1.7, there is two-pulse as a group for the first and second-mode when the pump power ratio is 1.85. Uniformly distributed pump power along the radius of the gain medium was assumed when the numerical calculations were performed, however, there were some variations of the pump power distribution inside the gain medium in the experiments. The environmental perturbations also have some effects on the measured pulse sequences for each mode. The transverse mode profile also has an effect on the antiphase states on the microchip lasers as discussed in reference [6]. The two-pulse group of the first-mode and second-mode in Figure 4 may be caused by the instability of the transverse mode, however, the total output pulse characteristics are not affected by this transverse mode instability. Although there are some simplifications in the numerical calculations, the numerical simulations of the antiphase states for the Cr,Yb:YAG self-Q-switched laser give us a clear image of the spatial hole burning of the gain medium and the nonlinear absorption of the saturable absorber on the dynamics of the antiphase states.

4 Conclusions

In conclusion, stable two-mode and three-mode oscillation in Cr,Yb:YAG self-Q-switched lasers were observed over a wide pump range. The stability of the output pulse trains was attributed to the mode coupling through antiphase dynamics. The antiphase dynamics of laser-diode-pumped Cr,Yb:YAG microchip self-Q-switched laser were investigated experimentally and numerically. The antiphase dynamics of this laser were investigated by separating the pulse sequences of each mode, the classical antiphase state of the two-mode oscillation and quasi-antiphase states of the three-mode oscillation were obtained experimentally. The numerical simulations based on the multimode passively Q-switched laser rate equations almost reproduced the observed antiphase dynamics of the two- and three-mode oscillation, and explained the antiphase dynamics of the Cr,Yb:YAG self-Q-switched laser. The stable antiphase states in compact microchip Cr,Yb:YAG self-Q-switched laser will be a promising source for secure information encoding and transmission.

This work was supported by the 21st Century Center of Excellence (COE) program of Ministry of Education, Science and Culture of Japan. J. Dong thanks Prof. P. Deng of Shanghai Institute of Optics and Fine Mechanics, Chinese Academy of Sciences for providing the Cr,Yb:YAG samples.

References

1. P. Hadley, M.R. Beasley, Appl. Phys. Lett. **50**, 621 (1987)
2. T. Baer, J. Opt. Soc. Am. B **3**, 1175 (1986)
3. K. Otsuka, Phys. Rev. Lett. **67**, 1090 (1991)
4. K. Otsuka, M. Georgiou, P. Mandel, Jpn J. Appl. Phys. **31**, L1250 (1992)
5. K. Otsuka, P. Mandel, M. Georgiou, C. Etrich, Jpn J. Appl. Phys. **32**, L318 (1993)
6. K. Otsuka, Jpn J. Appl. Phys. **32**, L1414 (1993)
7. M.A. Larotonda, A.M. Yacomotti, O.E. Martinez, Opt. Commun. **169**, 149 (1999)
8. Q. Zhang, B. Feng, D. Zhang, P. Fu, Z. Zhang, Z. Zhao, P. Deng, J. Xu, X. Xu, Y. Wang, X. Ma, Opt. Commun. **232**, 353 (2004)
9. E.A. Viktorov, P. Mandel, Opt. Lett. **22**, 1568 (1997)
10. J.J. Zayhowski, J. Alloys Comp. **303–304**, 393 (2000)
11. J. Dong, P. Deng, Y. Liu, Y. Zhang, G. Huang, F. Gan, Chin. Phys. Lett. **19**, 342 (2002)
12. J.J. Zayhowski, C. Dill III, Opt. Lett. **19**, 1427 (1994)
13. A.A. Lagatsky, A. Abdolvand, N.V. Kuleshov, Opt. Lett. **25**, 616 (2000)
14. G.J. Spuhler, R. Paschotta, M.P. Kullberg, M. Graf, M. Moser, E. Mix, G. Huber, C. Harder, U. Keller, Appl. Phys. B **72**, 285 (2001)
15. J. Dong, A. Shirakawa, S. Huang, Y. Feng, K. Takaichi, M. Musha, K. Ueda, A.A. Kaminskii, Laser Phys. Lett. **2**, 387 (2005)
16. J. Dong, M. Bass, Y. Mao, P. Deng, F. Gan, J. Opt. Soc. Am. B **20,** 1975 (2003)
17. S. Longhi, J. Opt. Soc. Am. B **11**, 1098 (1994)
18. G.K. Harkness, W.J. Firth, J. Mod. Opt. **39**, 2023 (1992)
19. W. Kochner, *Solid State Laser Engineering* (Springer-Verlag, Berlin, 1999)
20. C.L. Tang, H. Statz, G. Demars, J. Appl. Phys. **34**, 2289 (1963)
21. J. Dong, P. Deng, J. Lumin. **104**, 151 (2003)